International Communications in Heat and Mass Transfer 175 (2026) 111172

Contents lists available at ScienceDirect

International Communications in Heat and Mass Transfer

journal homepage: www.elsevier.com/locate/ichmt

Understanding Irreversible Processes in a Desiccant Wheel via Direct Entropy Generation Modeling

Jan Segura Schreiber *, Evgenia Makhova, Arne Speerforck

Institute of Engineering Thermodynamics, Hamburg University of Technology, Hamburg, Germany

ARTICLE INFO

Keywords:
Entropy
Desiccant wheel
Modelica
Second law
Ideal dehumidification
Non-equilibrium thermodynamics

ABSTRACT

This work presents for the first time a direct calculation of entropy generation mechanisms in a desiccant wheel (DW). A previously validated model is used to compute the entropy generated by various irreversible mechanisms. In addition, a clearly defined, idealized dehumidification process is proposed. The results show that irreversible heat transfer is the dominant source of entropy generation, accounting for about 40 % in the reference case. Mass transfer is the second-largest contributor, followed by dissipation and mixing. Comparison with the ideal process reveals that a large share of the system's exergy demand originates from irreversibilities within the DW itself, rather than from losses in the exhaust air streams. Parametric analysis of regeneration temperature and wheel rotational speed identifies operating conditions that minimize entropy generation. In addition, the temperature spread at the wheel outlet is found to be a reliable indicator of entropy generation. Local entropy generation analysis shows that optimal operating points exhibit a more dispersed distribution of entropy generation, whereas non-optimal points feature smaller dominant active zones at the boundary surfaces. These findings clarify the dominant loss mechanisms and provide practical guidance for improving the design and operation of desiccant wheels.

1. Introduction

The importance of air dehumidification in today's world cannot be understated. From industrial processes to the thermal comfort of people, air dehumidification plays a crucial role in many applications. As the need for air dehumidification increases and the energy supply of the world shifts towards renewable energy sources, the need for efficient air dehumidification processes is more important than ever [1].

Both in the realm of industrial and residential air conditioning, the energy required to dehumidify air is a significant portion of the total energy consumption. Especially in humid climates, the latent load is the primary factor in the energy consumption of air conditioning systems [2]. In the industrial sector, for example, one of the most energy intensive steps in the production of lithium-ion batteries is drying the air for the dry-room, consuming as much as 25 % to 50 % of the total energy demand of the process [3–5].

An effective approach to air dehumidification is the use of desiccant materials, which extract moisture from air without the need for cooling past the dew point. Especially for deep dehumidification requirements, this technique has the advantage of reaching low air humidity ratios without the need for sub-zero cooling. The key advantage of this method lies in separating the sensible and latent loads in the conditioning process, shifting the energy requirements from cooling the processed air to heating the regeneration stream used to regenerate the desiccant material [6,7]. Furthermore, the energy required to regenerate the desiccant material can be provided by low-exergy heat sources. Especially the integration with solar thermal collectors, waste heat or further sources of renewable energy is an important advantage to desiccant-assisted dehumidification [8–10].

1.1. Idealized processes and their real counterparts

As with any thermodynamic process involving using energy to achieve a certain goal, thermodynamic laws pose boundaries on the performance of a system. As in a work process, where the maximum work output is limited by the Carnot efficiency, the removal of moisture from a stream of air is also limited by the second law of thermodynamics. These limitations are bounded by an idealized process, with further limitations arising from irreversibilities present in a real process. Thus comparing the performance of a real process against an idealized one allows to quantify not the cost of operation from a perspective purely

* Corresponding author.
E-mail addresses: jan.segura.schreiber@tuhh.de (J. Segura Schreiber), e.makhova@tuhh.de (E. Makhova), arne.speerforck@tuhh.de (A. Speerforck).
URL: https://www.tuhh.de/itt (J. Segura Schreiber).

https://doi.org/10.1016/j.icheatmasstransfer.2026.111172

Nomenclature

Acronyms

CI	Confidence Interval
CV	Control Volume
DW	Desiccant Wheel
LHS	Left-Hand Side
PDS	Partial Dead State
RD	Regular Density
RHS	Right-Hand Side
TDS	Total Dead State

Roman Symbols

A	m^2	Surface Area
c	J/kgK	specific heat capacity (liquid)
c_p	J/kgK	specific isobaric heat capacity
c_v	J/kgK	specific isochoric heat capacity
d	m^2/s	diffusion coefficient
g	J/kg	specific Gibbs free energy
H	J	Enthalpy
h	J/kg	specific enthalpy
J	kg/m^2s	Species (diffusion) Flux
j	A/m^2	charge flux
J_q	W/m^2	Total Heat Flux
J'_q	W/m^2	Measurable heat flux
K	–	Equilibrium constant
L	m	Length
m	kg	Mass
n_{rot}	1/h	Rotational Speed
Nu	–	Nusselt-Number
p	Pa	pressure
Pr	–	Prandtl-Number
q	kg_w/kg_d	Sorbent water content
Q	J	Heat
R	J/kgK	Specific gas constant
r	mol/m^3s	rate of reaction
Re	–	Reynolds-Number
S	J/K	Entropy
s	J/kgK	specific entropy
Sh	–	Sherwood-Number
T	K	Temperature
t	s	time
U	J	Internal Energy
u	J/kg	specific internal energy
V	m^3	Volume
v	m^3/kg	specific volume
w	m/s	velocity
x	kg_w/kg_{DA}	Air moisture ratio/moisture content
x	m	spacial coordinate

Operators

$\dot{\square}$	flow variable/time derivative
$\Delta\square$	Change in ...
$\partial/\partial\square$	Partial derivative with respect to ...
$\sum_i \square_i$	Sum over all elements of ...

Greek Symbols

χ	kg_d/kg_r	rotor material mass ratio
$\delta_{\Delta p}$	–	Correction factor
μ	J/kg	specific chemical potential
ϕ	V	electric potential
ρ	kg/m^3	density
σ	J/m^3K	local entropy generation
φ	$\%_{RH}$	relative humidity
Ξ	J	Exergy
ζ	–	friction factor

Subscripts

0	Dead State
a, A	Air
adi	Adiabatic
c	Concentrate
conv	Convective
d	Desiccant Material
DA	Dry Air
dir	Direct
eff	Effective
eq	Equilibrium
f	Feed
gasMix	Substance Mixing
i, j	CV Coordinates
in	At Inflow Boundary
ind	Indirect
irr	Irreversible Entropy Generation
k	Species
m	Mass
max	Maximal
min	Minimal
mix	Mixing/Mixture
out	At Outflow Boundary
p	Partial
p	Product
pro	Process
Q	Heat
r	Rotor
ref	Reference
Reg/r	Regeneration
s	Solid
s	Saturation
s	Sorption
sep	Separation
thMix	Thermal Mixing
v	Vaporization
w	Water
Δp	Pressure Loss

centered on the cost-of-energy, but to quantify how "good" the process is compared to the theoretical maximum.

The concept of the least energy or work of separation is a concept well known in the field of chemical engineering, with common applications in the field of water treatment and carbon capture.

For example, Mistry and Lienhard [11] present a generalized thermodynamic analysis of the minimum energy of separation for the purpose of water desalination. Here, the authors present a generalized approach to calculate the minimum energy of separation for a generalized and idealized process, giving a lower bound for the energy input of a technically realizable desalination method (membranes, distillation, etc.). Caram et al. [12] show that the minimum work required to extract a certain amount of CO_2 from flue gas in a CCS-process is equal to the isothermal compression work required to compress the same amount of gas from its partial pressure to ambient conditions. Yuan and Rochelle [13] also give a method to calculate the minimum work required to separate a CO_2 stream from an amine solution. The minimum work of separation obtained by the authors mentioned above is obtained by the difference in the Gibbs free energy of the material streams before and after separation, assuming partial and total dead state conditions at the process boundaries. However, the concept of an idealized process for air dehumidification is not (consistently) defined in literature, thus not allowing to compare real dehumidification processes against an idealized one.

Seeing as dehumidification is similar to the above mentioned processes in the sense that a binary mixture is separated into two streams (product and concentrate), the concept of minimum energy of separation can be applied to dehumidification processes as well. As indicated by Mistry and Lienhard [11], the minimum work of separation can be obtained from an exergy balance of the system, assuming that the input and output streams are at the total or partial dead state. The total dead state is defined as the state of a fluid stream in thermal, mechanical and chemical equilibrium with its surroundings, while the partial dead state allows for chemical imbalance while maintaining thermal and mechanical equilibrium. The fact that for an idealized process all input and output streams are in thermal and mechanical equilibrium shows that in the ideal case dehumidification (or chemical separation in the general case) must be isothermal.

A comparison of the performance of the real (simulated) process against the ideal counterpart is then meaningful, as it allows to quantify the performance of the system against the maximum theoretical performance, taking into account the constraints imposed by thermodynamics. For the process presented in this paper, such a comparison is presented in the results section.

1.2. Second law analysis of dehumidification systems

Second law analysis of an energy system is a powerful tool to identify sources of irreversibility and to quantify the potential for improvement of the system. Especially in desiccant systems, where (coupled) heat and mass transfer processes take place, understanding these phenomena is crucial to improve system performance. The studies presented in the following sections, based on the second law of thermodynamics, study the constraints the second law imposes and the concepts that arise from it, such as exergy and entropy generation.

1.3. Review of exergy and entropy generation analyses

Exergetic analysis is widely used to study and evaluate the performance of air conditioning and dehumidification systems [14–16]. This type of analysis is based on the second law of thermodynamics and the concept that not all energy is convertible into useful work, or for the case of counter-clockwise-running cycles, a certain minimum amount of energy must be provided as work or as a heat flow with a certain temperature difference to the reference state (normally the environment). This minimum temperature difference is an indicator to where this energy can be sourced from: Processes with a low exergy requirement can be supplied with renewable, more accessible or less expensive energy sources, such as waste or solar heat, while processes with a high exergy requirement need to be supplied with high-quality energy sources, such as electricity, fossil- of biofuels.

Exergy analyses have been performed on desiccant dehumidification systems in the past, mainly focusing on an indirect calculation of exergy losses based on a reference state that is chosen arbitrarily and rarely matches between studies. For example, Ma et al. [17] presented an analysis of exergy losses differentiating between chemical and thermal exergy losses from transfer and mixing phenomena in a desiccant wheel system for conventional and deep dehumidification (the authors define deep dehumidification as reaching dew points below 0 °C or an air moisture content below $3.8\,g_w/kg_{DA}$). They find that the greatest exergy losses are caused by transfer phenomena in desiccant wheels with a 3:1 ratio of process to regeneration wheel face area ratios, and mixing losses rapidly increase with an increasing regeneration air moisture content. For the transfer losses, the authors state that the greatest exergy losses are of thermal nature. The authors do not consider pressure drop in the calculation of exergy losses.

Tu et al. [18] also conducted an exergy destruction analysis of a desiccant-wheel-based cooling system based on a simulation model. Exergy destruction is calculated for the desiccant wheel in an indirect way, balancing the exergy of the air streams entering and leaving it. The same method is used to calculate the exergy destruction in the other components of the desiccant cooling system (regeneration air heater, enthalpy recovery wheel and spray towers). It is found that (apart from exergy destruction in the electric heating unit) the greatest exergy destruction occurs in the desiccant and enthalpy recovery wheels, with the latter being the most significant source of exergy destruction. The high rate of exergy destruction of desiccant wheels is also reflected in other similar studies [19,20]. This indicates that heat and mass transfer phenomena in desiccant systems are the main sources of irreversibilities, as is reflected in the high exergy destruction rates in the components where these phenomena take place. Furthermore, mixing of inhomogeneous air streams is also a significant contributor to exergy destruction: Guan et al. [21] present an experimental and simulation-based investigation of the exergy destruction from mixing at the outlet of a DW. They find that for the analyzed scenarios, around 10 % of exergy is lost through mixing, and over 96 % of these losses arise from inhomogeneities in the tangential direction of the wheel, while those in radial direction are negligible. Furthermore, the authors find that the largest proportion of exergy losses are of thermal nature. These findings are similar to the investigations presented by Ma et al. [17], while the contribution of mixing to the total exergy losses presented by Tu et al. [22] presents larger variations.

In the studies mentioned above, exergy destruction is calculated in an indirect way by balancing the exergy of the substance streams at the system's control boundaries. Furthermore, the differentiation of exergy into thermal and chemical is only linked to the temperature and moisture content of the air streams (respectively) at the control boundaries, without considering how these two variables are affected by transfer phenomena. As such, the effect that – for example – water vapor adsorption and desorption (via mass transfer) has on the temperature of the air stream is only reflected in the thermal exergy, which is also affected by heat transfer. This approach thus does not allow to differentiate between the contributions of the transfer phenomena themselves.

As the amount of exergy contained in an energy stream depends on the reference state chosen to calculate it, the choice of a reference state is not trivial, especially when the reference temperature and the temperature of the process studied are close to each other [15,23]. In the context of buildings, the choice of a reference state and its meaning in terms of context is a topic of discussion [23,24]. Exergy destruction, however, is a concept that is directly linked to entropy generation, which is independent of the reference state chosen [25,26]. It only depends on the state of the media in the system, regardless of its surroundings and is linked to exergy destruction by Eq. (1):

$$\dot{\Xi}_{\mathrm{loss}} = T_0 \cdot \dot{S}_{\mathrm{irr}}, \tag{1}$$

where $\dot{\Xi}_{\mathrm{loss}}$ is the exergy loss, T_0 is the reference temperature and $\dot{S}_{\mathrm{irr}}$ is the entropy generation. Therefore, entropy generation can be used to evaluate the performance of an energy system in a more general sense and optimize it accordingly.

Previous studies have used entropy generation to analyze and optimize fluid flow and heat transfer phenomena [27,28]. For the performance of air conditioning systems, entropy generation has also been a valuable tool in previous studies: For example, Yang et al. [29] presented a local entropy generation analysis of an evaporative cooling system, where entropy generated through heat and mass transfer was used to select optimal operating conditions. Kocher et al. [30] also use entropy generation analysis to evaluate the performance of a thermoresponsive polymer-based dehumidification system, where the low entropy generation of the system is linked to its high efficiency.

Desiccant systems have also been analyzed regarding entropy generation. Giannetti et al. [31] analyzed the entropy generation in a desiccant wheel system from an analytical point using wheel effectiveness parameters for steady state operation, using an indirect approach to calculate entropy generation from heat and mass transfer. Similarly, Myat et al. [32] show that low entropy generation in a desiccant-based

multi-bed dehumidification system also leads to high efficiency. Guo et al. [33,34] also use local entropy generation analysis to evaluate the performance of a CO_2 capture process, where local entropy generation from transfer phenomena is calculated via CFD-Simulation.

Of the studies mentioned above, only Guo et al. [33,34], Yang et al. [29] differentiate entropy generation through heat and mass transfer in the system by source, while Myat et al. [32] presents the equations to calculate entropy generation from different sources, but does not present the contribution of each source separately in the results. These studies do not consider the contribution of mixing to total entropy generation.

The approach of Giannetti et al. [31] towards entropy generation is indirect, as it uses effectiveness parameters to calculate the entropy generation of the system rather than focusing on the transfer phenomena themselves. The approach of Kocher et al. [30] calculate entropy generation in the dehumidification system is also indirect. Furthermore, Kocher et al. [30], Myat et al. [32] use models that do not consider stream mixing from heterogeneous outlets from the cooling/desiccant system, so there is no consideration of the entropy generation from mixing.

To the best of the authors' knowledge, the literature does not yet present a comprehensive direct calculation of entropy generation within a desiccant wheel that accounts for transport phenomena and dissipation evaluated at the control-volume level, as well as the contributions from downstream flow mixing. In this paper, this novel type of analysis is presented in detail, where entropy generation through the various transfer phenomena is calculated directly from the transfer equations, allowing to identify the sources of irreversibilities in the system. The contribution of mixing and pressure drop to the total entropy generation is also presented, further widening the knowledge of irreversibility sources in desiccant wheels. Furthermore, as heat and mass transfer are local phenomena by nature, entropy generated form these sources is also calculated locally, not only allowing to identify how irreversible losses arise, but also where in the wheel they occur. The information gained from this new approach to the entropy sources in a desiccant wheel can therefore be used to optimize the design and operation of dehumidification systems.

2. Desiccant wheel modeling and entropy calculation

The model, its governing equations and the entropy generation methods are presented in the following sections.

2.1. Modeling of the desiccant wheel

The 2D finite volume element model analyzed in this work, implemented in the modeling language Modelica, was first introduced by Casas [35] and further developed and validated by various teams at Hamburg University of Technology [36,37]. The operation of the desiccant wheel is depicted as a two-dimensional (2D) finite-volume model discretized in the axial and tangential directions, resulting in control volumes (CVs) shaped like a slice of pizza. The CVs are divided into a solid and fluid part, between which heat and mass transfer phenomena take place, as shown in Fig. 1.

Both sides of the CV exhibit a mass flow rate $\dot{m}$ at the inflow and outflow boundaries, as well as the exchanged heat and mass flow rates $\dot{Q}$ and $\dot{m}_w$ between them. For the solid part, the mass flow rate $\dot{m}_r$ represents the wheel's rotational movement. The state of the fluid and solid parts of each CV is defined by the temperature T, the air humidity ratio x and the desiccant moisture content q. From these, energy and mass balances for each volume element are formulated. For the air part, these are given by [35]:

$$c_{p,a} \cdot V \cdot \rho \cdot \frac{\partial T}{\partial t} = \dot{H}_{in} + \dot{H}_{out} + \dot{Q}_{conv} + \dot{Q}_{conv,w} \tag{2}$$

and

$$V \cdot \frac{\partial \rho}{\partial t} = \dot{m}_{in} + \dot{m}_{out} + \dot{m}_w, \tag{3}$$

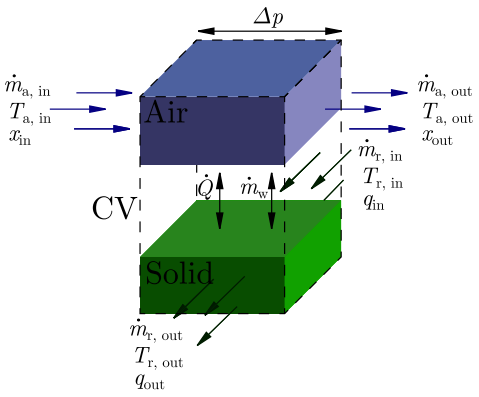

Fig. 1. Interface between solid and fluid control volumes.

where $c_{p,a}$ is the specific heat capacity of air, V is the volume of CV, ρ is the air density, $\dot{H}_{in}$ and $\dot{H}_{out}$ are the enthalpy flow rates at the inflow and outflow boundaries, $\dot{Q}_{conv}$ and $\dot{Q}_{conv,w}$ are the convective heat flow rates, and $\dot{m}_{in}$, $\dot{m}_{out}$ and $\dot{m}_w$ are the mass flow rates at the inflow and outflow boundaries and the mass flow rate of water vapor.[1]

For the solid side of the CV, the energy and water mass balances are given by [35]:

$$\begin{aligned}\frac{\partial U_r}{\partial t} &= \dot{Q}_{conv} + \dot{Q}_{conv,w} \\ &= \dot{Q}_{conv} + \dot{m}_w \cdot h_w,\end{aligned} \tag{4}$$

and

$$\frac{\partial m_w}{\partial t} = \dot{m}_w = m_r \cdot \chi \cdot \frac{\partial q}{\partial t}. \tag{5}$$

The state equation for the solid part of the CV is derived from Eq. (6):

$$\frac{\partial U_s}{\partial t} = \frac{\partial U_r}{\partial t} + \frac{\partial U_a}{\partial t}. \tag{6}$$

where U_s is the internal energy of the solid part of the control volume, which is the sum of the internal energies of the solid desiccant and rotor carrier materials U_r and the adsorbed water U_a. The internal energy of the adsorbed water is calculated from the enthalpy of adsorption h_s and the enthalpy of water vapor h_w [38]:

$$U_a = m_s \cdot \chi \cdot q \cdot u_a = m_s \cdot \chi \cdot q \cdot \left(h_w - h_s\right), \tag{7}$$

where $m_{w,a}$ is the mass of adsorbed water in the solid part of the control volume. The enthalpy of adsorption h_s is equal to the isosteric heat of adsorption. This leads to the formulation of the state equation for the solid part of the CV:

$$\frac{\partial u_s}{\partial t} = (c_s + \chi \cdot q \cdot c_{p,w}) \cdot \frac{\partial T}{\partial t} + \chi \cdot \left(\left(h_w - h_s\right) - q \cdot \frac{\partial h_s}{\partial q} \right) \cdot \frac{\partial q}{\partial t}, \tag{8}$$

where $c_s = (1 - \chi) \cdot c_r + \chi \cdot c_d$ is the specific heat capacity of the rotor carrier material and the solid desiccant and $c_{p,w}$ is the specific isobaric heat capacity of water vapor. The partial derivative of the enthalpy of adsorption $\partial h_s / \partial q$ is derived from the sorption heat data of the desiccant material.

The equations describing the calculation of exchanged heat flow, mass flow and pressure loss are presented in A.1 to A.3.

The equilibrium moisture content x_s is calculated by evaluating the sorption isotherm of the desiccant material,given in the general form:

$$\varphi_{eq} = \varphi_{eq}(q, T) \tag{9}$$

[1] Flow quantities (mass flow, heat flow, …) are defined as positive when entering a control volume and negative when leaving it. Therefore, all flow quantities have the same sign in the balance equations regardless of the CV boundary where they are evaluated.

where φ_{eq} is the equilibrium relative humidity for a given moisture content q and temperature T.

For the studied material (Silica Gel), the sorption isotherm is given by Pesaran and Mills [39] for regular density (RD) silica gel ($T_{ref} \approx 25°C$) in Eq. (10).

$$\varphi_{eq}(q) = 0.0078 - 0.05759\ q + 24.16554\ q^2 - 124.78\ q^3 + 204.226\ q^4 \quad (10)$$

The known sorption heat $h_s(q,T)$ is used to calculate the sorption isotherms at different temperatures through the Van't Hoff equation [40]:

$$\left(\frac{\partial \ln K}{\partial T}\right)_p = \frac{\Delta_r h^0(T)}{RT^2} \quad (11)$$

where $K = p_{p,w}/p_0$ is the equilibrium constant and $\Delta_r h^0(T) = h_s$ is the enthalpy of the reaction. Taking into account the enthalpy of vaporization given by the Clausius-Clapeyron equation (assuming ideal gas behavior and negligible liquid phase volume) [25]:

$$\frac{\partial \ln p_{s,w}(T)}{\partial T} = \frac{h_v}{RT^2} \quad (12)$$

(where $p_{s,w}(T)$ is the saturation pressure of water at a given Temperature T) a relationship between the equilibrium vapor pressure, the heat of vaporization, the enthalpy of sorption and the temperature can be established [41,42]:

$$\frac{h_s}{h_v(T)} = \left(\frac{\partial \ln(p_{eq}(T_{ref}, q))}{\partial \ln(p_{s,w}(T))}\right). \quad (13)$$

With the definition of the relative humidity $\varphi = p_{p,w}/p_{s,w}(T)$ the sorption isotherm for different temperatures can be expressed in its general form by integrating Eq. (13) and using the definition of relative humidity:

$$\varphi_{eq}(q,T) = \varphi_{eq}(q,T_{ref}) \cdot \left(\frac{p_{s,w}(T)}{p_{s,w}(T_{ref})}\right)^{\frac{h_s}{h_v(T)}}. \quad (14)$$

2.2. Entropy generation in heat and mass transfer processes

For systems where transfer phenomena (mass, heat and the coupling thereof) are driven by gradients in a potential quantity (temperature, pressure), entropy generation is inherent to the system. In general terms, the entropy generation rate σ at a local level for a one-dimensional[2] process assuming mechanical equilibrium is given by [44]:

$$\sigma = J_q \cdot \frac{\partial}{\partial x}\left(\frac{1}{T}\right) + \sum_k J_k \cdot \frac{\partial}{\partial x}\left(-\frac{\mu_k}{T}\right) + j\left(-\frac{1}{T}\frac{\partial \phi}{\partial x}\right) + r\left(-\frac{\Delta_r G}{T}\right), \quad (15)$$

where J_q is the (total) heat flux, J_k is the flux of species k, j is the flux of charge, r is the rate of reaction, μ_k is the chemical potential of species k, ϕ is the electric potential, $\Delta_r G$ is the Gibbs free energy of reaction and T is the temperature. The total irreversibilities can be obtained by the integration of the local entropy generation over the system volume:

$$\dot{S}_{irr} = \int_V \sigma\, dV. \quad (16)$$

In a desiccant wheel, chemical and charge equilibrium is assumed, which allows to neglect the last two terms of the Right-Hand-Side (RHS) of Eq. (15).

[2] The equations presented here, although valid for 3D-processes when considering further spacial dimensions, are presented here for a 1D-Process to avoid unnecessary burden. For a 3D-representation, the reader is referred to [43,44].

The total heat flux J_q is the sum of the measurable heat flux J'_q and the enthalpy transport:

$$J_q = J'_q + \sum_k J_k \cdot h_k, \quad (17)$$

where h_k is the enthalpy of species k [44,45].

Using the measurable heat flux J'_q and neglecting the aforementioned terms, the entropy generation rate σ simplifies to:

$$\sigma = \underbrace{J'_q\left(\frac{\partial}{\partial x}\frac{1}{T}\right)}_{\sigma_{Q,irr}} + \underbrace{\sum_k J_k\left(-\frac{1}{T}\frac{\partial \mu_{k,T}}{\partial x}\right)}_{\sigma_{m,irr}}, \quad (18)$$

with $\partial \mu_{k,T}/\partial x$ being the gradient of the chemical potential of species k at constant temperature.

The assumption of mechanical equilibrium does not hold in the context of desiccant wheels, especially when considering the tradeoff between pressure loss and heat/mass transfer efficacy. Therefore, the term shown in Eq. (19) to calculate entropy generation arising from pressure losses is added to Eq. (18):

$$\sigma_{\Delta p} = A \cdot w \cdot \frac{1}{T}\frac{\partial p}{\partial x}, \quad (19)$$

where A is the cross-sectional area, w is the fluid velocity and p is the pressure [46].

2.3. Simplifications and assumptions

In the context of desiccant wheels, assuming ideal gas behavior allows for further simplifications. Specifically, it is assumed that gases follow the ideal gas law and Dalton's law applies for the mixture of dry air and water vapor. These properties allow for the gradient of the chemical potential at constant temperature to be expressed as [44]:

$$\frac{1}{T}\frac{\partial \mu_{k,T}}{\partial x} = \frac{1}{T}\frac{\partial}{\partial x}(h(T) - Ts)\Big|_T = \frac{\partial}{\partial x}s. \quad (20)$$

Here, as the specific enthalpy $h(T)$ is a function of temperature only, the differential is zero and the gradient of the specific chemical potential is reduced to the gradient of the specific entropy $\partial s/\partial x$.

Furthermore, fluid heat conduction in flow direction and solid heat and mass conduction between CVs are neglected, and the solid is modeled as ideal in regard to mass transfer. It is assumed that all CVs of one rotor section (process/regeneration) have the same geometrical dimensions and that local mass transfer equilibrium applies at the boundary layer between fluid and solid. The moisture content of the fluid boundary layer is the equilibrium moisture content of the desiccant material for its given state.

2.4. Implementation of entropy calculation in the DW model

In the model presented here, four sources of entropy generation are considered: Heat transfer $\dot{S}_{Q,irr}$, mass transfer $\dot{S}_{m,irr}$, pressure loss $\dot{S}_{\Delta p}$ and stream mixing at the DW outlet surfaces $\dot{S}_{mix}$. The sum of these terms yields the total entropy generation rate for the DW via the direct method:

$$\dot{S}_{irr,dir} = \dot{S}_{Q,irr} + \dot{S}_{m,irr} + \dot{S}_{\Delta p} + \dot{S}_{mix}. \quad (21)$$

The first three sources of entropy generation are calculated at the CV level, while stream mixing is calculated downstream of the wheel. The discrete nature of the model calls for careful choice of evaluation points for state variables, especially for the calculation of gradients, which become differences in the discretized equations.

In order to visualize the calculation of heat and mass transfer entropy generation, a generalized control volume with two material streams (fluid and solid) shall be considered. The exchanged heat and mass flow from A to B, where A and B are the respective parts of the CV (solid or fluid, depending on the exchange direction). The inflow

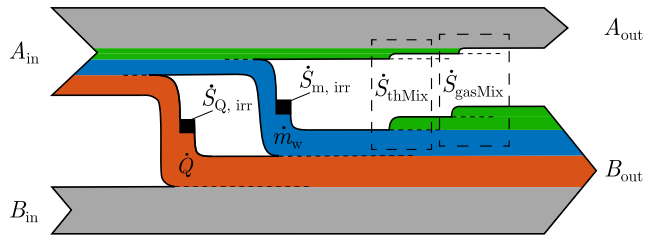

Fig. 2. Entropy flow and generation diagram for a Control Volume with two material streams that exchange heat and mass.

and outflow boundaries are denoted by the subscripts $\square_{in}$ and $\square_{out}$, respectively. The approach for the choice of evaluation points for state variables is illustrated with the help of Fig. 2.

The paths illustrated in Fig. 2 represent the entropy transfer and generation processes in the control volume. Heat and (direct) mass transfer (red and blue paths) lead to a decrease in entropy in the A part and an increase in entropy in the B part of the CV (entropy flow).

The net increase in entropy is the entropy generation $\dot{S}_{Q/m,irr}$ of the process, denoted by the black squares in the transfer paths. The green paths represent the change in entropy of the material that does not take part in the direct mass transfer process, but is still affected by it (as explained below). As with the transfer paths, the net positive entropy change along the green paths is also a factor in the overall entropy generation.

For the calculation of entropy generation arising from heat or direct mass transfer (the *transfer path*), the evaluation points for the state variables associated with these flows are set to the inflow and outflow points of the CV part where the flow starts(A_{in}) and ends (B_{out}), as per the definition above.

Not all of the material passing through the control volume participates in the mass transfer process (i.e. only some of the water vapor is adsorbed by the desiccant material, while the rest continues to flow). However, the water vapor that is not adsorbed is affected by the process, as its partial pressure changes due to the change in concentration. This change in partial pressure leads to a change in the specific entropy of the remaining water vapor (shown as the green paths in Fig. 2), which adds to the total entropy generation. The state variables for these non-participating flows are evaluated at the points where the flow enters and leaves the control volume (that is, at A_{in} and A_{out}). This form of entropy generation (the *flow path*) is associated with thermal and substance mixing processes.

The calculation method of these various sources of entropy are given in the following paragraphs.

2.4.1. Entropy generation from heat transfer

Entropy generation from heat transfer in a CV is defined by the heat flux and the temperature gradient along the transfer path, as expressed in Eq. (22):

$$\dot{S}_{Q,irr} = \dot{Q}_{AB} \cdot \left(\frac{1}{T_{B,out}} - \frac{1}{T_{A,in}} \right), \tag{22}$$

where $\dot{Q}_{AB}$ is the measurable heat flow rate from A to B, calculated in each CV with Eq. (38).

2.4.2. Entropy generation from mass transfer

Entropy generation due to mass transfer can be calculated by evaluating the second term on the RHS of Eq. (18) along the transfer and flow paths:

$$\dot{S}_{m,total,irr} = \sum_k J_k \left(-\frac{1}{T} \frac{\partial \mu_{k,T}}{\partial x} \right). \tag{23}$$

Evaluating this term for a CV along the transfer path yields the entropy generation due to direct mass transfer. As only water vapor is transferred, the calculation for air is omitted. As per the assumptions above, the gradient of the chemical potential at constant temperature is reduced to the gradient of the specific entropy, which can be calculated from the temperature and partial pressure of water vapor at the evaluation points.

This yields the entropy generation due to direct mass transfer along the transfer path:

$$\dot{S}_{m,direct,irr} = \dot{m}_{w,AB} \cdot \left(s_w \left(T_{B,w,in}, p_{p,B,out} \right) - s_w \left(T_{A,in}, p_{p,A,in} \right) \right), \tag{24}$$

where $T_{B,w,in}$ is the temperature of the inflowing water vapor stream ($\dot{m}_{w,AB}$) in the B part of the CV and $p_{p,B,out}$ and $p_{p,A,in}$ are the partial pressures of water vapor at the CV boundaries.

The temperature of water vapor is evaluated at the inflow boundary of the B part of the CV to separate the effect of thermal mixing from the direct mass transfer process. It is assumed that the driving force of mass transfer is the gradient in concentration between the main flow and the boundary layer, and that mass transfer is isothermal. It is only after arriving at the B part of the CV that the water vapor thermally mixes with the main flow, and the entropy generation due to this process is calculated separately.

Evaluating Eq. (23) in a CV along the flow path yields the entropy generation due to thermal and substance mixing, which arise indirectly from the mass transfer process. As stated above, the gradient of chemical potential at constant temperature is reduced to the gradient of the specific entropy, which for an ideal gas is given by Eq. (25) [25]:

$$s_2 - s_1 = c_p \cdot \ln\left(\frac{T_2}{T_1}\right) - R \cdot \ln\left(\frac{p_2}{p_1}\right), \tag{25}$$

where c_p is the specific heat capacity at constant pressure, R is the specific gas constant and T and p are the temperature and (partial) pressure, respectively. The first term on the RHS of Eq. (25) is the entropy change due to thermal mixing, while the second term is (in this case) the entropy change due to substance mixing. The sum of these two terms for all substances in the CV flow paths yields the entropy generated from indirect mass transfer.

When considering thermal mixing, the entropy produced must be calculated without the influence of conductive heat transfer. This is completed by calculating the adiabatic mixture temperature $T_{adi\,mix}$, which is the temperature of the material after water vapor has entered through the boundary layer and mixed with the main flow. This temperature is calculated according to Eq. (26):

$$T_{adi\ mix} = \frac{\dot{m}_{w,AB} \cdot c_{p,w} \cdot T_{w,in} + \dot{m}_B \cdot c_{B,in} \cdot T_{B,in}}{\left(\dot{m}_{w,AB} + \dot{m}_{B,in}\right) c_{B,out}}, \tag{26}$$

where $c_{B,in,in}$ and $c_{B,out}$ are the specific heat capacities of the main flow at the inflow and outflow boundaries of part B of the CV.

The adiabatic mixture temperature is then used to calculate the entropy generation due to thermal mixing:

$$\dot{S}_{th.\ mix} = \dot{m}_{w,AB} c_{p,w} \ln\left(\frac{T_{adi\ mix}}{T_{B,w,\ in}}\right) + \dot{m}_{B,in} c_{B,in} \ln\left(\frac{T_{adi\ mix}}{T_{B,\ in}}\right), \tag{27}$$

where $c_{B,in}$ is the specific heat capacity of the main flow at the inflow boundary of part B of the CV (calculated by the composition of the flow and the heat capacities of the components) and $c_{p,w}$ is the specific isobaric heat capacity of water vapor.

Entropy generation due to substance mixing is calculated by evaluating the second term of the RHS of Eq. (25) for all substances in the flow path:

$$\dot{S}_{gasMix} = \sum_k -\dot{m}_{k,flowpath} \cdot R_k \ln\left(\frac{p_{p,k,out}}{p_{p,k,in}} \cdot \delta_{\Delta p}\right) \tag{28}$$

where $\dot{m}_{k,flowpath}$ is the mass flow of substance k in the flow path (at the outflow of part A and inflow of part B of the CV) and R_k is the specific gas constant of substance k. The correction factor $\delta_{\Delta p}$ is introduced to correct for the pressure loss in the CV, as entropy generation due to

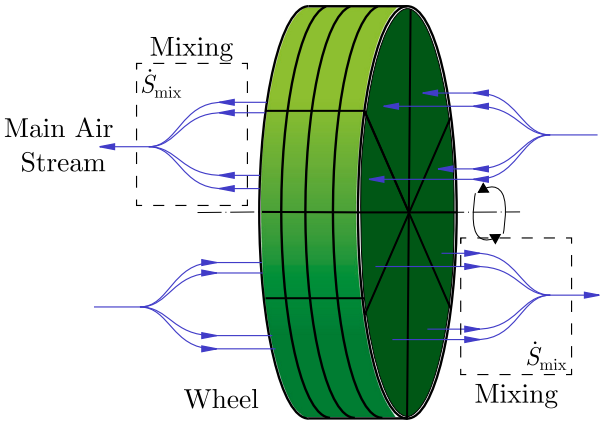

Fig. 3. Mixing of discrete streams into a homogenous stream.

pressure loss is calculated separately. It is defined as the inverse of the ratio of the pressure loss in the CV:

$$\delta_{\Delta p} = \frac{p_{\mathrm{in}}}{p_{\mathrm{out}}}, \tag{29}$$

which ensures only changes in partial pressure due to composition changes are considered in Eq. (28). This leads to the total entropy generation from mass transfer in a CV, expressed as the sum of direct and indirect mass transfer entropy generation:

$$\dot{S}_{\mathrm{m,irr}} = \dot{S}_{\mathrm{m,direct,irr}} + \dot{S}_{\mathrm{gasMix}} + \dot{S}_{\mathrm{th.mix}}. \tag{30}$$

2.4.3. Entropy of mixing downstream of the DW

Entropy generation in a sorptive process is not limited to the phenomena in the desiccant wheel. In a one-stage system, the entropy of mixing of the heterogenous air stream at the DW outflow surface into a homogenous one downstream of the wheel must be considered. For this, it is assumed that the air streams flowing out of the discrete screams resulting from the tangential discretization of the DW mix into a homogenous stream, as shown in Fig. 3.

The entropy of mixing is calculated by evaluating the specific entropy of the streams at their outflow state before and after mixture as expressed in Eq. (31):

$$\begin{aligned}\dot{S}_{\mathrm{mix}} &= \sum_{\mathrm{i}=1}^{\mathrm{m}} \left[\dot{m}_{\mathrm{i}} \left(s\left(T_{\mathrm{mix}}, x_{\mathrm{mix}}\right) - s\left(T_{\mathrm{i}}, x_{\mathrm{i}}\right)\right)\right] \\ &= \dot{m}_{\mathrm{total}}\, s\left(T_{\mathrm{mix}}, x_{\mathrm{mix}}\right) - \sum_{\mathrm{i}=1}^{\mathrm{m}} \dot{m}_{\mathrm{i}} s\left(T_{\mathrm{i}}, x_{\mathrm{i}}\right)\end{aligned} \tag{31}$$

2.4.4. Entropy generation from pressure loss

As stated in Eq. (19), irreversibilities due to pressure loss are calculated from the (total) pressure gradient in the fluid stream of the CV. Integrating the local entropy generation rate $\sigma_{\Delta p}$ over the control volume yields the total entropy generation due to pressure loss:

$$\dot{S}_{\Delta p} = \dot{V} \cdot \frac{1}{T} \cdot \Delta p, \tag{32}$$

where $\dot{V}$ is the volume flow rate of the fluid in the CV and Δp is the pressure loss, which is calculated as presented in Section 2.1. Further entropy sources are not considered.

3. Results

In this section, the results of the simulations performed with the desiccant wheel model are presented and discussed. First, the base case is presented to establish a baseline to compare the results of the other cases to. Then, the results of the sensitivity analysis are presented, where the influence of the wheel rotational speed and the regeneration air temperature on the entropy generation in the system is investigated. The minimal entropy generation for a given output air moisture content is presented and used to investigate the theoretical minimal regeneration air temperature for the system.

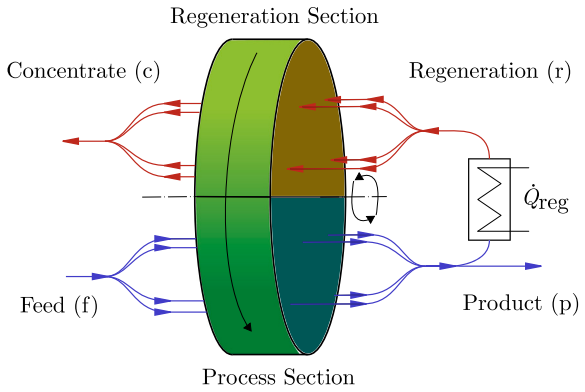

Fig. 4. Desiccant wheel process flow diagram.

Table 1
Reference case operational parameters.

Parameter	Value
Inlet (feed) air temperature T_{f}	9 °C
Inlet air moisture content x_{f}	7 g_w/kg_{DA}
Inlet air mass flow rate $\dot{m}_{\mathrm{f}}$	0.625 kg_{DA}/s
Regeneration air temperature T_{r}	60 °C
Regeneration air mass flow rate $\dot{m}_{\mathrm{r}}$	0.3125 kg_{DA}/s
Wheel rotational speed n_{rot}	6 rph

3.1. Simulation setup

Before analyzing the results of the simulations, an overview of the simulation setup is given. As explained before, the simulation of the desiccant wheel process is implemented in the software environment Dymola, a Modelica-based simulation environment.

The simulated process employs one rotating desiccant wheel, which is divided into two sections: Process and regeneration. The process section is fed with precooled feed air (subscript $_{\mathrm{f}}$), which is dehumidified as it passes through it. After the process section, a portion of the air is extracted as product air (subscript $_{\mathrm{p}}$), while the rest is fed into the regeneration section (subscript $_{\mathrm{r}}$). Before entering the regeneration section, the air is heated to a higher temperature by a heat exchanger. After reabsorbing the moisture from the desiccant material, the air is discharged into the environment.

A schematic of the desiccant wheel process is shown in Fig. 4.

3.2. Reference case

A number of simulations were performed with the DW model to investigate the behavior of entropy generation in the system. As a baseline, the reference case was simulated with the parameters listed in Table 1. The parameters are oriented on the conditions of the first stage of a multi-stage deep dehumidification desiccant system modeled by the authors for this study.

The simulated desiccant wheel was modeled using the geometrical and physical parameters listed in Table 2.

The simulation was run until a steady state was reached using the DASSL solver [47] to integrate the model DAE-System. The main results of the simulation are shown in Table 3. Absolute quantities are set in relation to the product air mass flow rate $\dot{m}_{\mathrm{p}} = \dot{m}_{\mathrm{f}} - \dot{m}_{\mathrm{c}}$.

As a comparison and accuracy check, the results of the entropy calculations via the control volume method are compared to an indirect

Table 2
Desiccant wheel parameters.

Parameter	Value
Diameter	0.87 m
Length	0.4 m
Desiccant material	RD Silica gel
Specific surface area	2700 m^2 m^{-3}
Hollow space fraction	0.82
Sinusoidal channel height	1.78 mm
Sinusoidal channel width	3.77 mm
Process air section angle	270°
Desiccant mass fraction χ	0.82
Axial CV Number	15
Tangential CV Number (process air)	24
Tangential CV Number (regeneration air)	8

Table 3
Reference case main results.

Quantity	Value
Processed air humidity ratio x_p	0.693 g_w/kg_{DA}
Processed air temperature T_p	26.47 °C
Regeneration Heat $\dot{Q}_{reg}/\dot{m}_p$	33.74 $kJ/kg_{DA,p}$
Discharge air temperature T_c	24.95 °C
Discharge air humidity ratio x_c	13.15 g_w/kg_{DA}
Entropy source	**Value [$kJ/kg_{DA,p}K$]**
Heat transfer $\dot{S}_{irr,Q}$	3.085
Mass transfer $\dot{S}_{irr,m}$	2.708
Pressure loss $\dot{S}_{irr,\Delta p}$	1.362
Stream mixing $\dot{S}_{irr,mix}$	0.6095
Total (direct method) $\dot{S}_{irr,dir}$	7.764
Total (Indirect method) $\dot{S}_{irr,ind}$	7.634

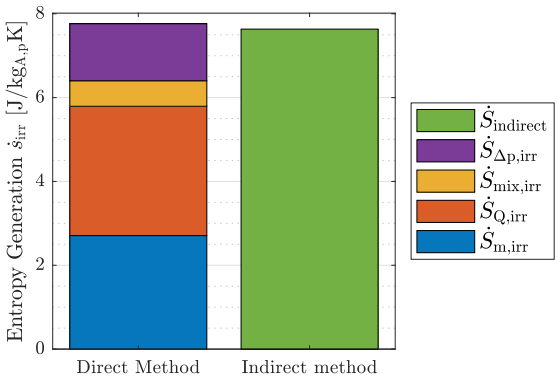

Fig. 5. Entropy generation by source for the reference case. The total entropy generation is calculated via the control volume method and via an indirect method.

calculation of the entropy generation via an entropy balance of the system:

$$\dot{S}_{irr,ind} = \sum_i \dot{m}_i s_i, \tag{33}$$

where $\dot{S}_{irr,ind}$ is the total entropy generation in the system, $\dot{m}_i$ are the mass flow rates of the streams i and s_i are the specific entropies of the streams at the control system boundary. The entropy generation rates by source and the total entropy generation calculation by the indirect method for the reference case are illustrated in Fig. 5.

In the reference scenario, the total entropy generation is dominated by the heat transfer entropy generation, which accounts for about 40 % of the entropy generated. It is followed closely by entropy generation from mass transfer, with pressure loss and stream mixing contributing to a lesser extent to the total entropy household. These results are in line with the findings of Ma et al. [17] and Guan et al. [21], which also found that transfer losses (heat and mass) are the largest contributors

Table 4
Operating points used to check the accuracy of the entropy generation calculations (C1 is the reference case).

Parameter	C1	C2	C3
x_f [g_w/kg_{DA}]	7	7	10
T_f [°C]	9	9	15
T_r [°C]	60	50	90
n_{rot} [rph]	6	40	10
Results			
x_p [g_w/kg_{DA}]	0.69	4.23	0.73
$\dot{S}_{dir}/\dot{S}_{ind} - 1$ [%]	1.71	2.67	−2.10

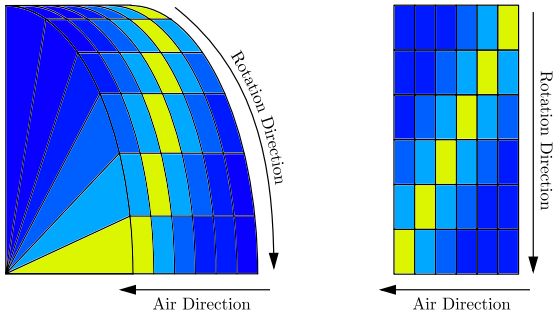

Fig. 6. Visualization of air stream and rotation directions.

to exergy losses (or entropy generation), and stream mixing accounts for roughly 20 % of exergy losses in the desiccant wheel system (when pressure loss is neglected) under similar operating conditions.

The difference between the entropy generation calculated by the direct and indirect methods has also been used as a measure of the accuracy of the implementation in similar systems by other authors [33, 34], where a relative difference in the calculated entropy generations under 3 % was qualified as good. The relative deviation reference case presented here lies at 1.71 %, which is considered very good. Further operating points were simulated to investigate the accuracy of the entropy generation calculations and the deviation between the direct and indirect methods. The main parameters of these simulated cases (also oriented on the operating conditions of the multiple stages of a dehumidification system) and the relative deviation between the two methods are presented in Table 4.

When considering the spacial distribution of entropy generation in the system, it can be seen that it is not evenly distributed over the wheel. As expected, entropy generation from heat and mass transfer is greatest at the wheel inlet surfaces, specifically at the points where the wheel material moves from the process section to the regeneration section and vice versa. This can be clearly seen in Fig. 7. The perspective on local entropy production heatmaps like Fig. 7 is of the flattened cylinder mantle of the desiccant wheel, with the air moving in the horizontal direction and the wheel rotating in the vertical direction (top to bottom), as visualized in Fig. 6.

Furthermore, entropy generation propagates in the direction of rotation and air flow, resulting in the diagonal “rays” seen in Fig. 7. This behavior can be explained by the fact that the “active zone” of the wheel, where the heat and mass transfer occurs, is also located along this diagonal. However it is worth noting that the active zones for heat and mass transfer are not identical.

In the direction of rotation, the process of heat transfer occurs prior to that of mass transfer. This is due to the initial heating or cooling of the wheel by the air, which results in a change to the equilibrium state and consequently drives the mass transfer process. In that sense, the amount of entropy generated by heat transfer is strongly related to heating or cooling the material to its equilibrium conditions for the respective air streams. As shown in Fig. 5, entropy generation is dominated by heat transfer, so the distribution of heat transfer entropy

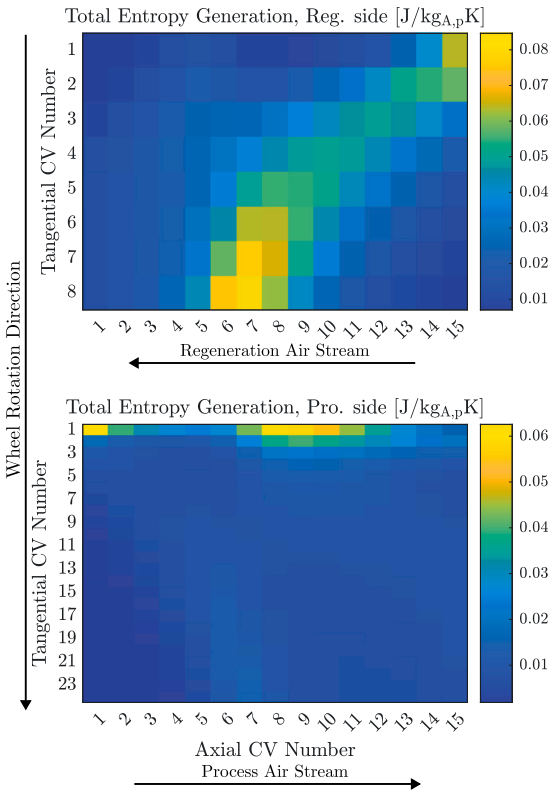

Fig. 7. Total entropy generation per control volume for the reference case. Top: Regeneration section, bottom: Process section.

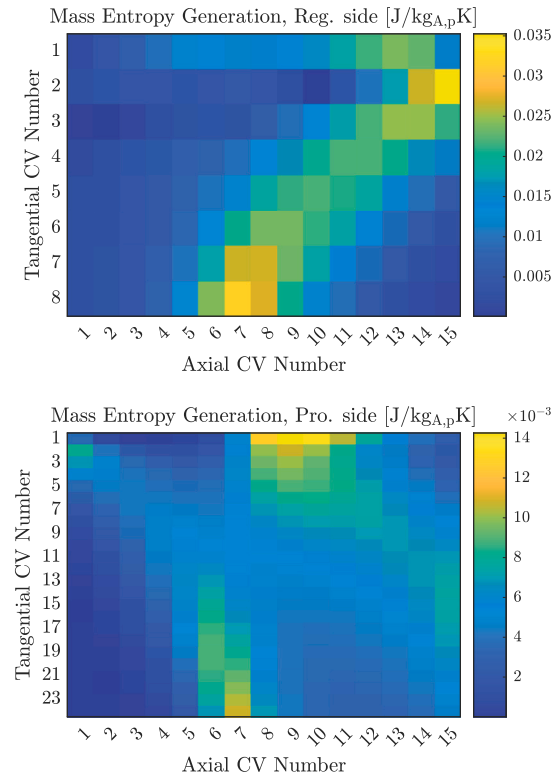

Fig. 8. Mass transfer entropy generation per control volume for the reference case. Rotation and air flow direction as in Fig. 7.

Table 5
Parameter ranges for the sensitivity analysis.

Parameter	Range
Wheel rotational speed	2 rph to 40 rph
Regeneration air temperature	40 °C to 100 °C

generation is very close to the total entropy generation presented in Fig. 7. Mass transfer entropy generation presents a more uniform propagation in rotation and air flow directions. This distribution can be seen in Fig. 8. Furthermore, it can be seen in Fig. 8 that the active zone for mass transfer propagates throughout the wheel, with the highest entropy generation occurring around CV (10, 1) in the process section and CV (7, 8) in the regeneration section. This finding suggests that the mass transfer process occurs over a greater surface area, thereby reducing the gradient in partial pressure necessary to transfer the desired amount of moisture and consequently decreasing entropy generation. Consequently, reduced entropy generation is indicative of a more efficient process.

3.3. Investigation of different operation points

The results of the reference case are used as a baseline to investigate the influence of different operation points on the entropy generation in the system. The parameters varied in the simulations are the wheel rotational speed and the regeneration air temperature, as these two parameters can be changed during operation with relative ease and have a significant influence on the performance of the system. Finding the optimal operation point however is not a trivial task, in which entropy analysis can be a useful tool. The investigated parameter ranges are shown in Table 5.

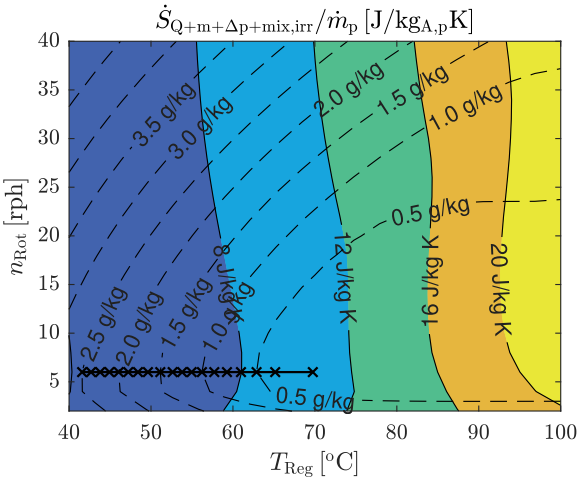

Fig. 9. Total entropy generation for the studied parameter range (colored), product air moisture ratio overlaid (in g_w/kg_A). Minimal entropy generation in an iso-*x*-line marked with crosses.

3.3.1. Total entropy generation

The total entropy generation is shown in Fig. 9 for the studied parameter range, with the product air moisture content overlaid.

As can be seen in Fig. 9, entropy generation is mainly dependent on the regeneration air temperature, although in the lower range the wheel rotational speed shows some influence. The reached product air moisture content is a function of both the wheel rotational speed and the regeneration air temperature and traverses a range of entropy generation states. However, there is always a point of minimal entropy generation along a given output moisture content isoline (iso-*x*-line). This point of minimal entropy generation is also the point where

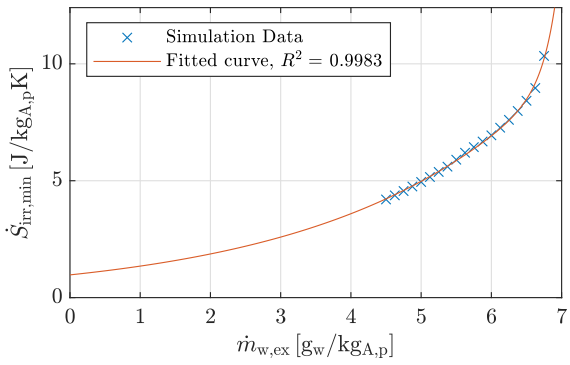

Fig. 10. Minimal entropy generation for various moisture extraction rates and fitted double exponential curve.

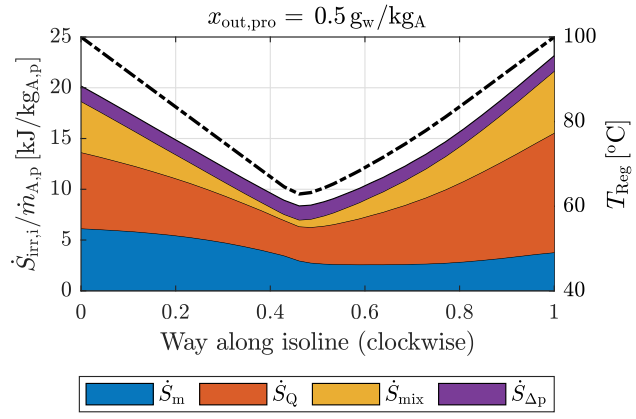

Fig. 11. Left Axis: Entropy generation by source along the 0.5g$_{\mathrm{w}}$/kg$_{\mathrm{A,p}}$ iso-x-line. Right axis: Regeneration air temperature (black, dashed).

a maximum moisture extraction is reached with the smallest regeneration temperature and the optimal wheel rotational speed (or the point of minimal output air moisture content for a given regeneration temperature).

This can be explained by the fact that when the wheel is operated at the optimal point, a greater portion of the wheel is active in regard to heat and mass transfer. This means that the necessary temperature and concentration gradients to achieve the same total heat and mass transfer are smaller, which results in less entropy generation.

As can be seen in Fig. 10, the amount of entropy generated at the point of minimal entropy generation increases exponentially with the amount of moisture extracted, indicating that the process will require significantly more exergy to reach very low moisture contents. This behavior is expected, as the necessary exergy of separation increases when separating water vapor from air at very low concentrations (see Section 3.3.3).

3.3.2. Composition of entropy generation

As shown for the reference case in Fig. 5, the total entropy generation can be decomposed into its components for further investigation. As one of the key output parameters of a dehumidification process is the product air moisture content, the entropy generation composition along an iso-x-line is to be analyzed.

Fig. 11 shows the entropy generation by source for the 0.5g$_{\mathrm{w}}$/kg$_{\mathrm{A,p}}$ iso-x-line, which is approximately the product air moisture content of the reference case. The line is swept clockwise, starting at the lower right and ending at the upper right corner of Fig. 9.

As can be seen in Fig. 11, pressure loss entropy generation is nearly constant along the iso-x-line, while the other components present

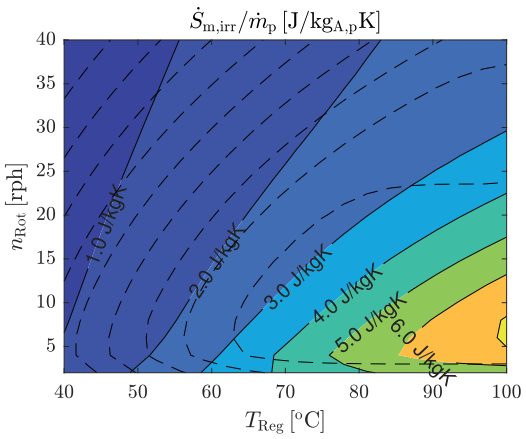

Fig. 12. Mass transfer entropy generation for different rotational speeds and regeneration air temperatures. Dashed: Iso-x-lines.

higher variation. Entropy generation from heat transfer is the largest component in all cases. Notable is that while entropy generation from heat transfer and stream mixing present a minimum at the point of minimal entropy generation, mass transfer entropy generation is smallest on the right side of the isoline, where the wheel rotational speed is highest. Entropy generation from stream mixing is at a minimum at the point of minimal entropy generation, indicating that the output air streams are in a more homogeneous state. Furthermore, at the point of minimal entropy generation, the mass transfer entropy generation is at an inflection point. The behavior of mass transfer entropy generation is similar to that of moisture extraction itself, i. e. the isolines of these two quantities are similar, as can be seen in Fig. 12.

The increased entropy generation at operating points away from the optimal point, characterized especially by the large contributions from heat transfer and mixing can again be attributed to the high temperature gradients across the CVs. When the regeneration temperature and rotational speed are not chosen optimally, the active zones in the wheel are smaller, leading to higher entropy generation.

When analyzing spacial distribution of mass entropy generation, it can be seen that in the point of minimal entropy generation the active zone for mass transfer is spread out across the wheel, while in a point with greater entropy generation the active zone is located at the interface between the process and regeneration sections, as shown in Fig. 13.

The distribution of mass transfer entropy along the output surface of the desiccant wheel in Fig. 13 shows that there is significant heterogeneity in the wheel output, which in turn leads to a higher amount of entropy produced by the mixing of the air streams exiting the wheel channels. This is reflected in the fact that at the start and end of an iso-x-line, entropy generation from mixing is higher than at the optimal point.

A low entropy of mixing also indicates a good match between the regeneration temperature and the wheel rotational speed, leading to larger active zones, which imply a relatively uniform temperature and moisture content distribution at the wheel output surface. The temperature and moisture content distribution at the wheel process side output surface for the optimal point and a point of increased entropy generation is shown in Fig. 14.

As expected, both distributions show a lower spread between the maximum and minimum values at the point of minimal entropy generation, while the spread is larger at the point of increased entropy generation. Looking closer at the distribution of moisture content and temperature, it can be seen that output moisture content can be closely expressed as a function of the output temperature, as shown in Fig. 15.

This fact can be used to estimate the moisture content distribution at the wheel output surface from the temperature distribution

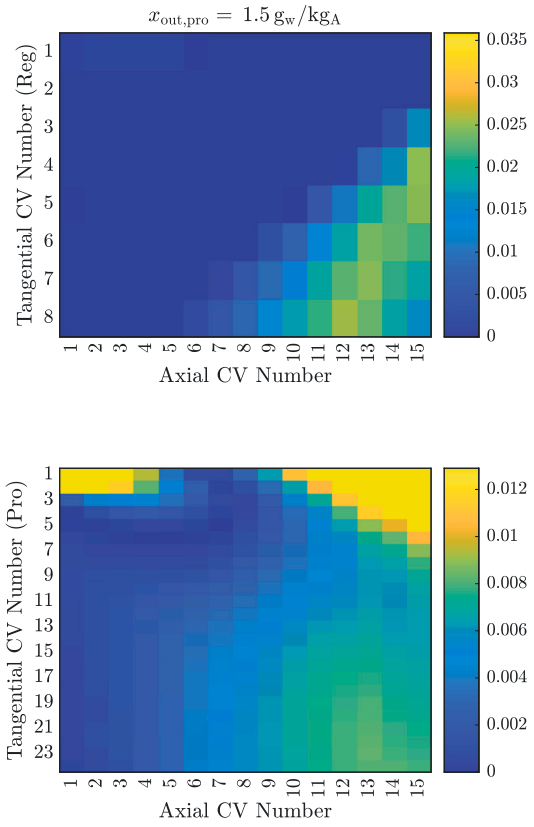

Fig. 13. Mass transfer entropy generation per control volume for a point of increased entropy generation (x_p = 1.5 $g_w/kg_{DA,p}$, n_{rot} = 40 rph and T_{Reg} = 90 °C). Rotation and air flow direction as in Fig. 7.

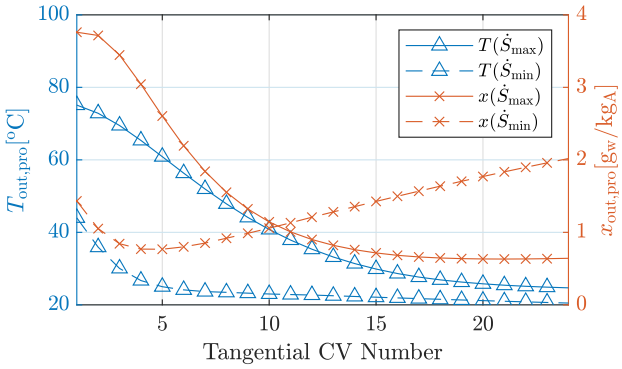

Fig. 14. Temperature and moisture content distribution at the wheel process side output surface for a point of minimal and increased (conditions presented in Fig. 13) entropy generation, x_p = 1.5 g_w/kg_{DA}.

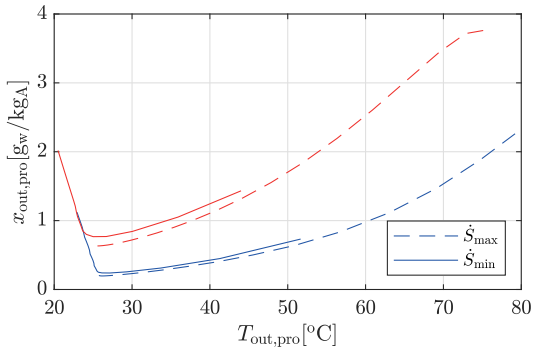

Fig. 15. Local air moisture content as a function of local output temperature (process side) for x_p = 0.5 $g_w kg^{-1}_{DA}$ (blue) and 1.5 $g_w kg^{-1}_{DA}$ (red) at the minimum (solid) and increased (dashed) entropy generation points. (For interpretation of the references to color in this figure legend, the reader is referred to the web version of this article.)

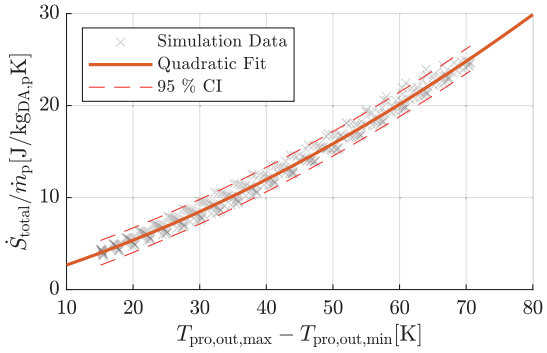

Fig. 16. Total entropy generation against process air temperature spread across the simulated operation points, quadratic fit and 95% confidence interval.

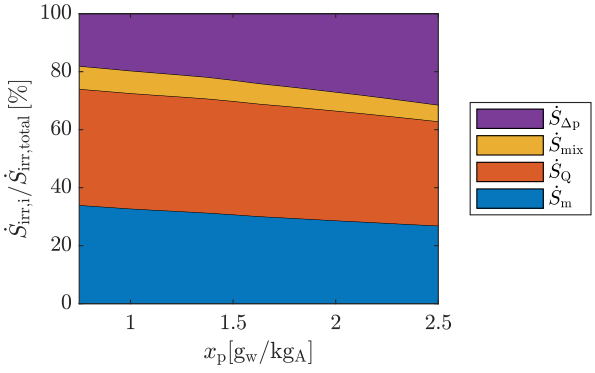

Fig. 17. Entropy generation by source along the line of minimal entropy generation.

(temperature spread), which can be measured e. g. with a thermal camera.

Using this information, aiming to achieve a uniform temperature distribution (or a low temperature spread) at the wheel output surface can be used as a control strategy to minimize the entropy generation in the system, as the temperature distribution is directly related to the amount of entropy of mixing generated in the system, which in turn is similar to the total entropy generation.

The correlation between total entropy generation and the process air temperature spread is shown in Fig. 16.

As can be seen in Fig. 16, the correlation between total entropy generation and process air temperature spread shows that total entropy generation rises quadratically with the output temperature spread, which makes measuring this temperature spread a good indicator of how close the system is to the optimal operating point.

Following the line of minimal entropy generation (from Fig. 9), it can be seen that the relative contribution of mixing and heat and mass transfer to the total entropy generation varies lightly, while the contribution from pressure loss presents larger variations, as shown in Fig. 17.

It implies that, under optimal conditions, the heat input is balanced with the demand of the dehumidification process driven by mass transfer, ensuring that no additional heat is recirculated into the process

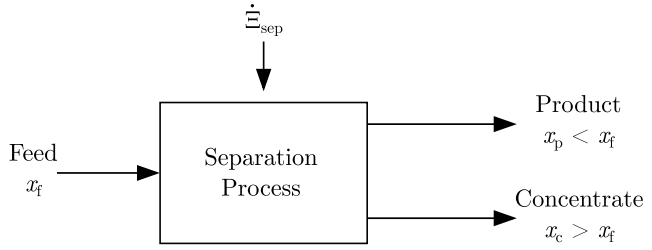

Fig. 18. Idealized separation process diagram (based on [11]).

air that would eventually be lost to the environment. As expected, the relative contribution of pressure loss increases with the output moisture content, as the absolute amount is nearly constant for the different operation points and the total entropy generation is smaller for higher product air moisture contents.

3.3.3. Comparison with an ideal separation process

As shown in the previous sections, the fact that entropy is generated in the dehumidification process means that it is not reversible and a certain amount of exergy is lost. In order to investigate how much more exergy is required to achieve a certain output state, an idealized process is used to compare the results of the desiccant wheel process to. The idealized process is defined as a separation process where the only energy input is the minimum exergy of separation, as defined by Mistry and Lienhard [11] and presented in Fig. 18. As mentioned in Section 1.1, this process is isothermal in the ideal case, as all material streams enter and exit the process at the dead state temperature T_0.

The least of exergy of separation is derived from an exergy balance of the inlet and outlet process streams (feed $\dot{m}_f$, product $\dot{m}_p$ and concentrate $\dot{m}_c$). Furthermore, it is assumed that the exergy input is provided by the regeneration air stream $\dot{m}_r$, which is heated to the regeneration temperature T_{Reg}.

The exergy of separation is obtained from the process exergy balance, given by Eq. (34):

$$\dot{\Xi}_{sep} = \dot{\Xi}_r = \underbrace{\dot{\Xi}_f - \dot{\Xi}_p - \dot{\Xi}_c}_{\text{Exergy Streams}} + \underbrace{T_0 \dot{S}_{irr}}_{\text{Exergy Destruction}}. \tag{34}$$

The exergy streams $\dot{\Xi}_i$ are defined as [25]:

$$\dot{\Xi}_i = \dot{m}_i \left(h_i - h_{0,i} - T_0(s_i - s_{0,i})\right) \tag{35}$$

$$= \dot{m}_i \left(g_i - g_{0,i}\right), \tag{36}$$

where $h_i = h(T_i, x_i, p_i)$ and $s = s(T_i, x_i, p_i)$ are the specific enthalpy and entropy of the stream, respectively, and $h_{0,i}$ and $s_{0,i}$ are the specific enthalpy and entropy at the dead state. The least exergy (or work) of separation is obtained by assuming that the process is reversible, there is no entropy generation, the output streams are at the partial dead state (PDS), and the feed stream is at the total dead state (TDS) and the process is at a steady state. As the reference state, the conditions of the feed air stream are used, which simplifies the exergy balance to

$$\frac{\dot{\Xi}_{sep}}{\dot{m}_p} = (g_p - g_c) - \frac{1}{r}(g_f - g_c) + T_0 \frac{\dot{S}_{irr}}{\dot{m}_p}, \tag{37}$$

where $r = \dot{m}_p/\dot{m}_f$ is the recovery ratio and g_i is the specific Gibbs free energy of the stream evaluated at reference temperature T_0 [11].

The minimum exergy of separation for the studied output moisture content is shown in Fig. 19.

The exergy of separation for the irreversible cases is calculated with the minimal entropy generation shown in Fig. 10 and the corresponding output moisture content. Two irreversible cases are considered: the first is the case where the output streams are at the PDS, and the second is the case where the output streams are at the simulated output conditions. In the second case, the exergy carried by the output streams

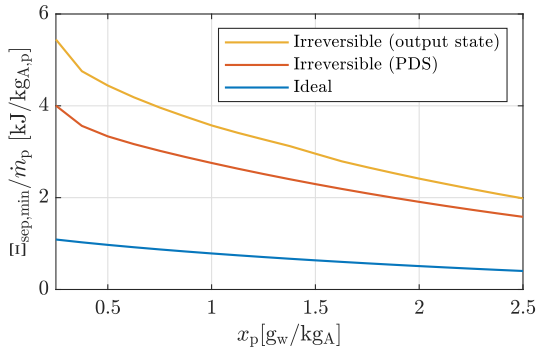

Fig. 19. Minimum exergy of separation in the ideal and irreversible cases (output at PDS and at simulated output conditions).

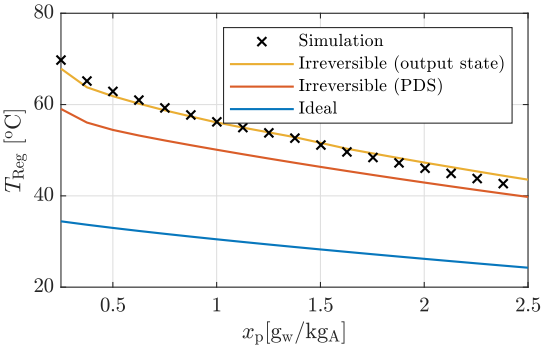

Fig. 20. Regeneration air temperature for the ideal and irreversible cases shown in Fig. 19 and simulation results.

is considered, further raising the exergy requirements of the separation process. Knowing the least exergy of separation, the regeneration air temperature can be calculated, as the regeneration air stream must carry the exergy of separation shown in Fig. 19. For the studied output moisture content, the necessary regeneration air temperature (obtained by solving Eq. (35) numerically) is shown in Fig. 20.

As can be seen in Fig. 20, the necessary regeneration temperature for the irreversible case with the streams at output conditions closely matches the regeneration temperatures used in the simulation, which speaks for the accuracy of the calculation methods. Furthermore, the regeneration temperature for the ideal case is significantly lower than the regeneration temperature for the irreversible cases, with the entropy generation alone accounting for the greatest difference between the ideal and real (simulated) cases. The exergy lost to the environment through the output air streams, while also significant, contributes only to small part of the temperature increase required to drive the process.

4. Conclusion and outlook

The results of the implementation of entropy generation in the desiccant wheel model allow for a deeper understanding of the thermodynamic limitations of a desiccant-assisted air dehumidification system.

The following key findings can be summarized from the results:

- Entropy generation is dominated by heat transfer irreversibilities, which denotes the large effect of the temperature swing needed to drive adsorption and desorption (it shall be noted that with other wheel geometries, pressure loss could play a larger role or dominate entropy generation). Heat transfer should be the first target to reduce entropy generation.

Table 6
Coefficients for the friction factor correlation (Eq. (42)) [48].

i	c_i	d_i
0	$3.9696 \cdot 10^{-2}$	0
1	5.5194	$1.6134 \cdot 10^{-1}$
2	$-5.4847 \cdot 10^{1}$	$5.1725 \cdot 10^{1}$
3	$1.2819 \cdot 10^{2}$	$2.0336 \cdot 10^{2}$
4	–	$-8.9791 \cdot 10^{2}$

- Entropy generation rises exponentially with lower output air moisture contents, raising exergy requirements in a similar manner.
- In an optimal operation point, entropy (especially from mass transfer) is generated along the volume of the desiccant wheel, rather than at the boundary surfaces between sections and to the incoming air streams.
- A large amount of the exergy input is destroyed by entropy generation, rather than being lost through the exhaust air.
- In order to reduce the exergy requirements, efforts should focus on reducing entropy generation before increasing energy recovery from exhaust air streams.
- During operation, a minimum of entropy generation can be reached by monitoring and minimizing the temperature spread on the desiccant wheel outlet surface.
- The state of minimal entropy generation for a given regeneration temperature is reached when the product air moisture content is at a minimum.

As mentioned before, the model is limited by the assumption that moist air behaves as an ideal gas, which brings some uncertainty to the results. However, the main conclusions of the work remain valid, as this assumption does not affect the qualitative behavior of the entropy generation sources and their relative importance. Furthermore, the transient behavior of the system was not considered, which could present further optimization opportunities for the operation of the system.

Further efforts in the optimization of desiccant-assisted air dehumidification systems should use these findings to optimize their design and improve operation. Especially the design of control strategies and systems can benefit from entropy generation analysis in order to reach operation points with minimal entropy generation for the set product air conditions.

CRediT authorship contribution statement

Jan Segura Schreiber: Writing – original draft, Methodology, Formal analysis, Conceptualization. **Evgenia Makhova:** Methodology, Funding acquisition, Conceptualization. **Arne Speerforck:** Writing – review & editing, Validation, Methodology, Funding acquisition.

Declaration of Generative AI and AI-assisted technologies in the writing process

During the preparation of this work, the authors used GitHub Copilot and DeepL Write for aid in document readability and document typesetting. After using this tool, the authors reviewed and edited the content as needed and take full responsibility for the content of the published article.

Declaration of competing interest

The authors declare the following financial interests/personal relationships which may be considered as potential competing interests: Jan Segura Schreiber reports article publishing charges was provided by Project DEAL. Jan Segura Schreiber reports financial support was provided by Hamburgische Investitions- und Förderbank. If there are other authors, they declare that they have no known competing financial interests or personal relationships that could have appeared to influence the work reported in this paper.

Acknowledgments

This research was supported by the Investment and Development Bank Hamburg (Hamburgische Investitions- und Förderbank IFB) under Grant 51171605. The Article Processing Charge (APC) was funded by Project DEAL.

Appendix. Calculation of heat and mass transfer and pressure loss for each CV

The equations to calculate heat and mass transfer and pressure loss in the CVs of the DW model are presented here.

A.1. Heat transfer

The heat flow rate that arises from convection in the fluid $\dot{Q}_{\mathrm{conv}}$ is calculated from

$$\dot{Q}_{\mathrm{conv}} = A_{\mathrm{eff}} \cdot \mathrm{Nu} \cdot \frac{\lambda_a}{L} \cdot (T_{\mathrm{a}} - T_{\mathrm{s}}), \tag{38}$$

where A_{eff} is the effective heat transfer area, λ_a is the thermal conductivity of air and L is a characteristic length (hydraulic diameter of the wheel canals) and Nu is the Nusselt-number, obtained from the work of Kakaç et al. [49]. The convective heat flow rate $\dot{Q}_{\mathrm{conv,w}}$ is given by:

$$\dot{Q}_{\mathrm{conv,w}} = \dot{m}_{\mathrm{w}} \cdot h_{\mathrm{w}}, \tag{39}$$

where h_{w} is the specific enthalpy of water vapor.

A.2. Mass transfer

Mass transfer is calculated from

$$\dot{m}_{\mathrm{w}} = \mathrm{Sh} \cdot \frac{d}{L} \cdot \rho \cdot A_{\mathrm{eff}} \cdot (x_{\mathrm{a}} - x_{\mathrm{s}}), \tag{40}$$

where Sh is the Sherwood-number, d is the diffusion coefficient, L is a characteristic length and x_{s} is the air equilibrium moisture content at the desiccant boundary layer. The Sherwood number is obtained from the work presented by Schirmer [50].

A.3. Pressure loss

Pressure loss Δp is calculated from friction factor correlations:

$$\Delta p = \frac{1}{2} \rho w^2 \cdot \zeta, \tag{41}$$

where ρ is the density of the fluid, w is the velocity of the fluid and ζ is the friction factor. It is obtained from the correlations presented by Yamaguchi and Saito [48]:

$$\zeta\ \mathrm{Re} = 52.96 + \sum_{i=0}^{3} c_i \left(\frac{L/d_h}{\mathrm{Re}} \right)^i / \sum_{i=0}^{4} d_i \left(\frac{L/d_h}{\mathrm{Re}} \right)^i \tag{42}$$

where L is the rotor length and d_h is the hydraulic diameter of the channel. The coefficients c_i and d_i are listed in Table 6.

Data availability

Data will be made available on request.

References

[1] M. Abdelgaied, M.A. Saber, M.M. Bassuoni, A.M. Khaira, Adsorption air conditioning: A comprehensive review in desiccant materials, system progress, and recent studies on different configurations of hybrid solid desiccant air conditioning systems, Environ. Sci. Pollut. Res. 30 (11) (2023) 28344–28372, http://dx.doi.org/10.1007/s11356-023-25209-z.

[2] L.G. Harriman, D. Plager, D. Kosar, Dehumidification and Cooling Loads From Ventilation Air, Energy Eng. 96 (6) (1999) 31–45, http://dx.doi.org/10.1080/01998595.1999.10530479.

[3] F. Degen, M. Winter, D. Bendig, J. Tübke, Energy consumption of current and future production of lithium-ion and post lithium-ion battery cells, Nat. Energy 8 (11) (2023) 1284–1295, http://dx.doi.org/10.1038/s41560-023-01355-z.

[4] M. Schütte, F. Degen, H. Walter, Reducing Energy Consumption and Greenhouse Gas Emissions of Industrial Drying Processes in Lithium-Ion Battery Cell Production: A Qualitative Technology Benchmark, Batteries 10 (2) (2024) 64, http://dx.doi.org/10.3390/batteries10020064.

[5] C. Yuan, Y. Deng, T. Li, F. Yang, Manufacturing energy analysis of lithium ion battery pack for electric vehicles, CIRP Ann 66 (1) (2017) 53–56, http://dx.doi.org/10.1016/j.cirp.2017.04.109.

[6] B. Guan, T. Zhang, X. Liu, On-site performance investigation of a desiccant wheel deep-dehumidification system applied in lithium battery manufacturing plant, Energy Build. 232 (2021) 110659, http://dx.doi.org/10.1016/j.enbuild.2020.110659, URL https://www.sciencedirect.com/science/article/pii/S0378778820334459.

[7] M.N. Golubovic, H.D.M. Hettiarachchi, W.M. Worek, Evaluation of rotary dehumidifier performance with and without heated purge, Int. Commun. Heat Mass Transfer 34 (7) (2007) 785–795, http://dx.doi.org/10.1016/j.icheatmasstransfer.2007.03.011, URL https://www.sciencedirect.com/science/article/pii/S0735193307000644.

[8] M. Sultan, I.I. El-Sharkawy, T. Miyazaki, B.B. Saha, S. Koyama, An overview of solid desiccant dehumidification and air conditioning systems, Renew. Sustain. Energy Rev. 46 (2015) 16–29, http://dx.doi.org/10.1016/j.rser.2015.02.038.

[9] A. Speerforck, G. Schmitz, Experimental investigation of a ground-coupled desiccant assisted air conditioning system, Appl. Energy 181 (2016) 575–585, http://dx.doi.org/10.1016/j.apenergy.2016.08.036, URL https://www.sciencedirect.com/science/article/pii/S0306261916311230.

[10] D. Pandelidis, S. Anisimov, W.M. Worek, P. Drąg, Numerical analysis of a desiccant system with cross-flow Maisotsenko cycle heat and mass exchanger, Energy Build. 123 (2016) 136–150, http://dx.doi.org/10.1016/j.enbuild.2016.04.039, URL https://www.sciencedirect.com/science/article/pii/S0378778816302948.

[11] K. Mistry, J. Lienhard, Generalized Least Energy of Separation for Desalination and Other Chemical Separation Processes, MDPI Publ. (2013) URL https://dspace.mit.edu/handle/1721.1/80326.

[12] H.S. Caram, R. Gupta, H. Thomann, F. Ni, S.C. Weston, M. Afeworki, A simple thermodynamic tool for assessing energy requirements for carbon capture using solid or liquid sorbents, Int. J. Greenh. Gas Control. 97 (2020) 102986, http://dx.doi.org/10.1016/j.ijggc.2020.102986, URL https://www.sciencedirect.com/science/article/pii/S1750583619306607.

[13] Y. Yuan, G.T. Rochelle, Lost work: A comparison of water-lean solvent to a second generation aqueous amine process for CO2 capture, Int. J. Greenh. Gas Control. 84 (2019) 82–90, http://dx.doi.org/10.1016/j.ijggc.2019.03.013, URL https://www.sciencedirect.com/science/article/pii/S1750583618307084.

[14] A. Hepbasli, Low exergy (LowEx) heating and cooling systems for sustainable buildings and societies, Renew. Sustain. Energy Rev. 16 (1) (2012) 73–104, http://dx.doi.org/10.1016/j.rser.2011.07.138.

[15] G. Streckienė, V. Martinaitis, J. Bielskus, From Entropy Generation to Exergy Efficiency at Varying Reference Environment Temperature: Case Study of an Air Handling Unit, Entropy 21 (4) (2019) 361, http://dx.doi.org/10.3390/e21040361.

[16] I. Dincer, M. Rosen, Exergy Analysis of Heating, Refrigerating and Air Conditioning: Methods and Applications, Elsevier, Amsterdam, [Netherlands], 2015.

[17] Z. Ma, X. Liu, B. Guan, T. Zhang, Exergy destruction comparison of facial area ratio on dehumidification performance of the rotary desiccant wheel system under conventional and deep dehumidification, Appl. Therm. Eng. 234 (2023) 121293, http://dx.doi.org/10.1016/j.applthermaleng.2023.121293, URL https://www.sciencedirect.com/science/article/pii/S1359431123013224.

[18] R. Tu, X.H. Liu, Y. Hwang, F. Ma, Performance analysis of ventilation systems with desiccant wheel cooling based on exergy destruction, Energy Convers. Manage. 123 (2016) 265–279, http://dx.doi.org/10.1016/j.enconman.2016.06.013, URL https://www.sciencedirect.com/science/article/pii/S0196890416304927.

[19] İ. Uçkan, T. Yılmaz, E. Hürdoğan, O. Büyükalaca, Exergy analysis of a novel configuration of desiccant based evaporative air conditioning system, Energy Convers. Manage. 84 (2014) 524–532, http://dx.doi.org/10.1016/j.enconman.2014.05.006, URL https://www.sciencedirect.com/science/article/pii/S0196890414004178.

[20] M. Yari, F. Meulany, S. Mahmoudi, Thermodynamic analyses of advanced desiccant cooling systems with various configurations, Int. J. Exergy 13 (1) (2013) 36, http://dx.doi.org/10.1504/IJEX.2013.055777, URL http://www.inderscience.com/link.php?id=55777.

[21] B. Guan, Y. Liu, J. Zhang, X. Chang, T. Zhang, X. Liu, Enhancing exergy performance: Addressing air parameters nonuniformity at the outlet cross-section in desiccant wheel air-conditioning, Appl. Therm. Eng. 258 (2025) 124672, http://dx.doi.org/10.1016/j.applthermaleng.2024.124672, URL https://www.sciencedirect.com/science/article/pii/S1359431124023408.

[22] R. Tu, X.H. Liu, Y. Jiang, Lowering the regeneration temperature of a rotary wheel dehumidification system using exergy analysis, Energy Convers. Manage. 89 (2015) 162–174, http://dx.doi.org/10.1016/j.enconman.2014.09.068, URL https://www.sciencedirect.com/science/article/pii/S0196890414008693.

[23] V. Bonetti, Dynamic exergy analysis for the built environment: Fixed or variable reference? in: S. Nižetić, P. Šolić, Željka. Milanović (Eds.), Proceedings of the 9th Exergy, Energy and Environment Symposium, Split, Croatia, 2017, pp. 924–939.

[24] D. Schmidt, H. Torío (Eds.), Exergy Assessment Guidebook for the Built Environment: ECBCS Annex 49 - Low Exergy Systems for High-Performance Buildings and Communities, Fraunhofer Verlag, Stuttgart, 2011.

[25] G. Schmitz, Technische Thermodynamik, 11. Auflage ed., Vulkan Verlag, Essen, 2022.

[26] P. Stephan, K. Schaber, K. Stephan, F. Mayinger, Thermodynamik: Grundlagen und technische Anwendungen Band 1: Einstoffsysteme, 19. Aufl. 2013, in: Springer-Lehrbuch, Springer Berlin Heidelberg, Berlin, Heidelberg, 2013, http://dx.doi.org/10.1007/978-3-642-30098-1.

[27] T. Hayat, A. Razzaq, S.S. Jamal, A. Razaq, S.A. Khan, Entropy generation assessment in radiative rheological nanomaterial beyond conventional approach of heat and mass fluxes, Case Stud. Therm. Eng. 73 (2025) 106669, http://dx.doi.org/10.1016/j.csite.2025.106669, URL https://www.sciencedirect.com/science/article/pii/S2214157X25009293.

[28] T. Wenterodt, H. Herwig, The Entropic Potential Concept: A New Way to Look at Energy Transfer Operations, Entropy 16 (4) (2014) 2071–2084, http://dx.doi.org/10.3390/e16042071, URL https://www.mdpi.com/1099-4300/16/4/2071.

[29] C. Yang, H. Chen, T. Miyazaki, Y.-D. Kim, R. Khargotra, K. Thu, Local Entropy Generation Analysis of the Counter-Flow Dew-Point Evaporative Coolers, ASME J. Eng. Sustain. Build. Cities 5 (021004) (2024) http://dx.doi.org/10.1115/1.4065740.

[30] J.D. Kocher, S.K. Yee, R.Y. Wang, A first and second law analysis of a thermoresponsive polymer desiccant dehumidification and cooling cycle, Energy Convers. Manage. 253 (2022) 115158, http://dx.doi.org/10.1016/j.enconman.2021.115158, URL https://www.sciencedirect.com/science/article/pii/S0196890421013340.

[31] N. Giannetti, A. Rocchetti, K. Saito, S. Yamaguchi, Entropy parameters for desiccant wheel design, Appl. Therm. Eng. 75 (2015) 826–838, http://dx.doi.org/10.1016/j.applthermaleng.2014.10.025.

[32] A. Myat, K. Thu, N.K. Choon, The experimental investigation on the performance of a low temperature waste heat-driven multi-bed desiccant dehumidifier (MBDD) and minimization of entropy generation, Appl. Therm. Eng. 39 (2012) 70–77, http://dx.doi.org/10.1016/j.applthermaleng.2012.01.041, URL https://www.sciencedirect.com/science/article/pii/S1359431112000609.

[33] Z. Guo, S. Deng, S. Li, Y. Lian, L. Zhao, X. Yuan, Entropy Analysis of Temperature Swing Adsorption for CO2 Capture Using the Computational Fluid Dynamics (CFD) Method, Entropy 21 (3) (2019) 285, http://dx.doi.org/10.3390/e21030285.

[34] Z. Guo, S. Deng, Y. Zhu, L. Zhao, X. Yuan, S. Li, L. Chen, Non-equilibrium thermodynamic analysis of adsorption carbon capture: Contributors, mechanisms and verification of entropy generation, Energy 208 (2020) 118348, http://dx.doi.org/10.1016/j.energy.2020.118348.

[35] W. Casas, Untersuchung und Optimierung sorptionsgestützter Klimatisierungsprozesse, 1. Aufl ed., Cuvillier, Göttingen, 2005.

[36] J. Wrobel, P. Morgenstern, G. Schmitz, Modeling and experimental validation of the desiccant wheel in a hybrid desiccant air conditioning system, Appl. Therm. Eng. 51 (1) (2013) 1082–1091, http://dx.doi.org/10.1016/j.applthermaleng.2012.09.033.

[37] A. Speerforck, J. Ling, V. Aute, R. Radermacher, G. Schmitz, Modeling and simulation of a desiccant assisted solar and geothermal air conditioning system, Energy 141 (2017) 2321–2336, http://dx.doi.org/10.1016/j.energy.2017.11.151.

[38] T.L. Hill, Statistical Mechanics of Adsorption. V. Thermodynamics and Heat of Adsorption, J. Chem. Phys. 17 (6) (1949) 520–535, http://dx.doi.org/10.1063/1.1747314.

[39] A.A. Pesaran, A.F. Mills, Moisture transport in silica gel packed beds—II. Experimental study, Int. J. Heat Mass Transfer 30 (6) (1987) 1051–1060, http://dx.doi.org/10.1016/0017-9310(87)90035-4.

[40] P. Stephan, K. Schaber, K. Stephan, F. Mayinger, Thermodynamik: Grundlagen und technische Anwendungen - Band 2: Mehrstoffsysteme und chemische Reaktionen, Springer, Berlin, Heidelberg, 2017, http://dx.doi.org/10.1007/978-3-662-54439-6, URL http://link.springer.com/10.1007/978-3-662-54439-6.

[41] D.J. Close, P.J. Banks, Coupled equilibrium heat and single adsorbate transfer in fluid flow through a porous medium — II Predictions for a silica-gel air-drier using characteristic charts, Chem. Eng. Sci. 27 (5) (1972) 1157–1169, http://dx.doi.org/10.1016/0009-2509(72)80026-5, URL https://www.sciencedirect.com/science/article/pii/0009250972800265.

[42] M.J. Goldsworthy, Measurements of water vapour sorption isotherms for RD silica gel, AQSOA-Z01, AQSOA-Z02, AQSOA-Z05 and CECA zeolite 3A, Microporous Mesoporous Mater. 196 (2014) 59–67, http://dx.doi.org/10.1016/j.micromeso.2014.04.046.

[43] Y. Jin, E. Makhova, A. Speerforck, Optimization of Packed-Bed Energy Storage Systems Based on a Second Law Analysis, 2026, http://dx.doi.org/10.48550/arXiv.2601.13329, arXiv:2601.13329.

[44] S. Kjelstrup, D. Bedeaux, E. Johannessen, J. Gross, Non-Equilibrium Thermodynamics for Engineers, World scientific, Singapore, 2010.

[45] C.G. Carrington, Z.F. Sun, Second law analysis of combined heat and mass transfer phenomena, Int. J. Heat Mass Transfer 34 (11) (1991) 2767–2773, http://dx.doi.org/10.1016/0017-9310(91)90235-7.

[46] C. Carrington, Z. Sun, Second law analysis of combined heat and mass transfer in internal and external flows, Int. J. Heat Fluid Flow 13 (1) (1992) 65–70, http://dx.doi.org/10.1016/0142-727X(92)90060-M.

[47] L.R. Petzold, Description of DASSL: A Differential/Algebraic System Solver, Technical Report SAND-82-8637; CONF-820810-21, Sandia National Labs., Livermore, CA (USA), 1982, URL https://www.osti.gov/biblio/5882821.

[48] S. Yamaguchi, K. Saito, Numerical and experimental performance analysis of rotary desiccant wheels, Int. J. Heat Mass Transfer 60 (2013) 51–60, http://dx.doi.org/10.1016/j.ijheatmasstransfer.2012.12.036, URL https://linkinghub.elsevier.com/retrieve/pii/S0017931012009921.

[49] S. Kakaç, R.K. Shah, W. Aung (Eds.), Handbook of single-phase convective heat transfer, in: A Wiley-Interscience Publication, Wiley, New York, 1987.

[50] R. Schirmer, Die Diffusionszahl von Wasserdampf- Luft-Gemischen Und Die Verdampfungsgeschwindigkeit, VDI-Verlag, 1938.